Interfacial Interactions in Silica-Reinforced Polypropylene Nanocomposites and Their Impact on the Mechanical Properties

Diego Pedrazzoli,[1,2] Alessandro Pegoretti,[1] Kyriaki Kalaitzidou[2,3]
[1]*Department of Industrial Engineering and INSTM Research Unit, University of Trento, Trento 38123, Italy*

[2]*G. W. Woodruff School of Mechanical Engineering – Georgia Institute of Technology, Atlanta, Georgia 30336*

[3]*School of Materials Science and Engineering, Georgia Institute of Technology, Atlanta, Georgia 30322*

The main focus of this study is to characterize the interfacial interactions between silica nanoparticles and polypropylene and to investigate how the surface properties and morphology of the silica nanoparticles affect the elastic response of the silica–polypropylene composites. The composites were prepared by melt compounding and injection molding. Both non-functionalized and dimethyldichlorosilane-functionalized silica nanoparticles were used. Three-component composites were also prepared by including selected formulations of both poly(propylene-*g*-maleic anhydride) copolymer (PPgMA) and different types of silica. It was found that both silica types are nucleating agents for PP and significantly alter its crystallization behavior. A strong correlation between the glass transition temperature (T_g) and the tensile modulus in silica-PP nanocomposites indicated the presence of a secondary reinforcing mechanism that is the pinning of the polymer chains on the silica surface. The presence of a complex constrained phase, represented by immobilized amorphous and transcrystalline phases, forming at the filler surface, was assessed by modulated differential scanning calorimetry and dynamic mechanical analysis. Finally, the interfacial interactions were correlated to the tensile and viscoelastic properties using the theoretical models proposed by Pukanszky and Sumita et al., respectively, and comparing the predictions of the models to experimental results. POLYM. COMPOS., 37:2018–2026, 2016.
© 2015 Society of Plastics Engineers

INTRODUCTION

A novel class of materials, namely the polymer nanocomposites, has recently shown new and novel properties thanks to the addition of nanostructured materials such as fumed silica, carbon nanotubes, and graphite nanoplatelets. An advantage of nanocomposites over traditional micro-reinforced composites is that thanks to the extremely high surface area of nanofillers, an improvement of the mechanical and thermomechanical properties [1–3], gas barrier properties, and thermal and electrical conductivity [4, 5] can be achieved at low filler contents (less than 5 wt%). However, the unique properties of the nano-reinforcements cannot be fully exploited in nanocomposites because of agglomeration and weak interfacial interactions that result in reduced stress transfer at the reinforcement–polymer interface [6, 7]. In particular, interfacial interactions represent an important issue, as polar nanofillers (such as silicas, metal oxides, layered silicates, etc.) are generally poorly dispersed in apolar thermoplastics (such as polyolefins), thus limiting the improvement of the thermomechanical properties. To enhance the dispersability of nanofillers in polyolefins, they are usually added after appropriate surface treatment or together with a polymeric compatibilizer.

Interfacial interactions are important in micro-reinforced composites, but they really play a dominant role in case of nanocomposites, determining the dispersion and agglomeration of the filler within the matrix and the stress transfer along the interface, which dictate the physical properties of the polymer matrix and consequently the macroscopic characteristics of the nanocomposite [8, 9]. The recent literature highlights the need of considering various experimentally observed filler characteristics such as aspect ratio [10, 11], agglomerate size, and presence and properties of interphase [12, 13] to develop better design tools to fabricate multifunctional polymer composites. In particular, it is of great interest to understand how nanoscale interfacial interactions affect the macroscale properties in polymer nanocomposites [14, 15].

Present research has been mainly focused on the understanding of the mechanisms involved in the polymer chain dynamics upon nanofiller modification. In

Correspondence to: D. Pedrazzoli; e-mail: pedrazzoli.diego@gmail.com
DOI 10.1002/pc.23380
Published online in Wiley Online Library (wileyonlinelibrary.com).
© 2015 Society of Plastics Engineers

particular, it has been shown that the interfacial interactions in polymer nanocomposites lead to significant changes in the physical properties of the polymer, including glass transition [16], viscoelastic behavior, and crystallization behavior [17, 18]. Moreover, the presence of a constrained amorphous phase located not only at the crystal surface but also at the filler surface has been confirmed and, as reported, it induces secondary reinforcing mechanisms which, in addition to the primary stiffening effect due to the high modulus of the filler particles, significantly contribute to the enhancement of the bulk properties of semicrystalline polymer composites [19].

On the other hand, few studies have been dedicated to the modeling of the relationships between the macroscopic mechanical properties of nanocomposites and their interfacial interactions which are expressed usually in terms of the interfacial shear strength. Pukanszky developed a model to predict the variation of the composite's yield stress with the filler content, introducing a parameter that accounts for the interfacial interactions [20, 21]. Sumita et al. [22] used the information obtained from dynamic mechanical analysis (DMA) measurements to estimate the effective volume fraction of the dispersed phase. Also in this case, a parameter is introduced to describe the interfacial interactions. Shang et al. [23] proposed another model that correlates the work of adhesion, which is related to the interfacial interactions, with the elastic modulus and the tensile strength in silica-filled polymer composites.

Therefore, the main aim of this study is to provide better understanding on the impact of interfacial interactions on the physical characteristics of the polypropylene (PP) matrix and in turn on the macroscopic mechanical performance of silica-reinforced PP nanocomposites. The thermomechanical properties of the polymeric matrix characterized as a function of the silica content and type are used to reveal the relationships among interfacial interactions, tensile properties, and viscoelastic behavior in silica PP composites. The experimental results are compared with theoretical models that relate the interfacial interactions to macroscopic mechanical properties. To generate different interfacial interactions, both untreated and silane-treated silica particles are used to produce the materials under investigation.

EXPERIMENTAL

Materials and Composites Preparation

The matrix of the nanocomposites used in this work was an isotactic homopolymer polypropylene (MFI at 190°C and 2.16 kg = 6.9 g/10 min, density = 0.904 g/cm^3) produced by Polychim Industrie S.A.S. (Loon-Plage, France) and provided by Lati Industria Termoplastici S.P.A (Varese, Italy) with the commercial code PPH-B-10-FB. Maleic anhydride modified polypropylene (PPgMA) (Fusabond® P M-613-05, MFI at 190°C and 2.16 kg = 106.8 g/10 min, density = 0.903 g/cm^3, maleic anhydride content = 0.35–0.70 wt%), was supplied by DuPont™ de Nemours (Geneva, Switzerland). Both untreated and surface-treated fumed silica nanoparticles were supplied by Evonik Industries AG (Hanau, Germany). Untreated nanoparticles (Aerosil® A380), indicated as S_u, had an average primary particle size of 7 nm and a specific surface area of 321 ± 3 m^2/g, as determined by BET analysis [24]. Dimethyldichlorosilane functionalized silica nanoparticles (Aerosil® R974), designated as S_t, had an average primary particle size of 12 nm and a BET-specific surface area of 124 ± 1 m^2/g.

The nanocomposites were produced by melt mixing and injection molding. A vertical, co-rotating, bench-top twin-screw micro-extruder (DSM Micro 15 cm^3 Compounder) connected to a micro-injection molding unit (DSM) were used. The compound was mixed for 3 min, at 190°C, and a screw speed of 250 rpm. The temperature of the mold was 80°C, whereas the injection molding pressure was about 800 kPa. Ternary nanocomposites were prepared by adding 5 wt% of PPgMA as a compatibilizer to the systems containing 5 wt% of silica.

Composites are designated indicating the matrix, the compatibilizer (if any) with its content, the kind of filler with its amount. For instance, a composite containing 5 wt% of PPgMA and 5 wt% of Aerosil® A380 is indicated as PP-PPgMA-5-S_u−5.

Experimental Techniques

Fracture surfaces of nanocomposite specimens were observed using a Zeiss Ultra60 (Carl Zeiss NTS GmbH - Germany) field emission scanning electron microscope (FE-SEM), at an acceleration voltage of 5 kV. Before the SEM observations, a thin gold coating was applied onto the surface by plasma sputtering to minimize the charging effects.

Standard differential scanning calorimetry (DSC) and modulated DSC tests were performed at a DSC Q2000 (TA Instruments, New Castle, Delaware) under a constant nitrogen flow of 50 ml/min. The samples were heated up from the equilibrated temperature of 0–200°C at 5°C/min followed by cooling down to 0°C, at 5°C/min. During heating and cooling a modulation of ±1°C every 60 s was adopted to decompose the total heat flow signal into reversing (describing heat capacity events including the glass transition and melting) and nonreversing information (related to kinetic events such as crystallization and crystal perfection).

Uniaxial ramp tensile tests were performed with an Instron model 33R 4466 (Norwood) tensile tester equipped with a 500-N load cell at a crosshead speed of 5 mm/min. Values of the elastic modulus and yield stress were determined recording the load and the axial strain by using a resistance extensometer Instron® model 2630-101 with a gauge length of 10 mm. As indicated by the ISO527 standard, an elastic modulus was determined on

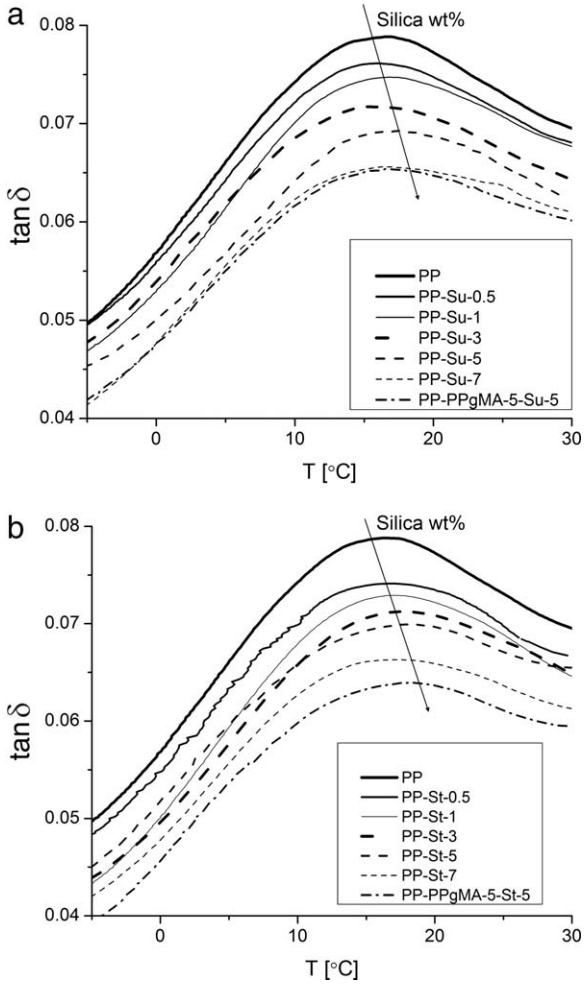

FIG. 1. Tan δ of (a) PP-S_u and (b) PP-S_t composites as a function of temperature and filler amount.

the stress–strain curves as a secant value between longitudinal deformations of 0.05 and 0.25%. Each data point reported is an average of five tests. Dynamic mechanical analyses (DMA) were performed in tensile mode on a DMA Q800 (TA Instruments, New Castle, Delaware) testing machine over a temperature range between −20 and 160°C, imposing a heating rate of 5°C/min at a frequency of 1 Hz. A preload of 0.2 MPa and a maximum strain of 0.05% were imposed on rectangular samples 25 mm long, 3.30 mm wide, and 3.27 mm thick.

RESULTS AND DISCUSSION

Interfacial Interactions and Constrained Polymer Phase

Interfacial interactions in PP-based nanocomposites represent an important issue, because polar nanofillers including silica are generally poorly dispersed in apolar thermoplastics (such as polyolefins), thus limiting the improvement of the thermomechanical properties. To enhance the dispersability of nanofillers in polyolefins, they are usually added after appropriate surface treatment or together with a polymeric compatibilizer.

The interfacial interactions were assessed by experimental determination of the viscoelastic properties, including the glass transition temperature, T_g, storage modulus, and tan δ and the crystallization behavior in terms of crystallization temperature T_c, and degree of crystallinity χ, as a function of the silica type and content.

Specifically, as shown in Fig. 1, the tan δ peak value decreases and shifts toward higher temperatures as the silica content increases which means that the composites become stiffer and the T_g increases [19] (Table 1). The increase in T_g indicates that the polymer chains are pinned on the silica surface. These constrained polymer chains also contribute to an increase in stiffness providing a secondary reinforcing mechanism. The question whether these immobilized polymer chains are amorphous or crystalline will be addressed in the crystallization study that follows. It is also noted that the stiffening effect and the increase in T_g is larger in the case of the treated silica particles which is expected, because the treated particles will result in stronger interfacial interactions. Furthermore, the difference in tan δ and T_g between the untreated and surface-treated silica-reinforced composites, for the same silica content, clearly demonstrates that the viscoelastic properties correlate strongly to the interfacial interactions and that the stronger the interactions the larger the constrained polymer phase at the silica surface, which means the secondary reinforcing mechanism becomes more dominant.

To decouple the two different reinforcing mechanisms, the stiffening caused by the presence of the stiffer silica particles which dominates the elastic behavior at temperatures below T_g, and the stiffening caused by the constrained polymer phase at the silica surface which will contribute to the elastic behavior of the composites at temperatures above T_g, the storage modulus of the silica nanocomposites, normalized with respect to that of neat PP, above and below T_g, is presented as a function of the filler content in Fig. 2. The normalized storage modulus (E_c'/E_m') is higher for both PP-S_u and PP-S_t composites when considered above T_g than when evaluated below T_g. This would not have been the case if the stiffening was only due to the addition of the stiffer silica particles. Therefore, this behavior is attributed to the polymer chains which are pinned at the silica surface forming the constrained and stiffer phase mentioned earlier. Noteworthy, the pinning of polymer chains depends on the available filler surfaces and this quantity is dependent upon the agglomeration degree. Another possible explanation is that addition of silica increases the degree of crystallinity in the polymer and, as it is known, the crystalline regions are stiffer that the amorphous ones.

In addition to using surface-treated silica particles to enhance the interfacial interactions, PP*g*MA compatibilizer was also used in 5 wt% silica composites with both

 DOI 10.1002/pc

TABLE 1. Crystallization and viscoelastic properties of the silica nanocomposites.

Sample	$\chi_{\%}$[a]	Tan δ_{Tg}[b]	T_g (°C)[c]	$C_{\%}$[d]	$(C\text{-}\chi)_{\%}$[e]	Brittleness[f] 10^{10}/(%·Pa)
PP	41.8 ± 0.2	0.0789 ± 0.0010	15.05 ± 0.11	41.8	0.0	0.018
PP-S_u −0.5	41.4 ± 0.3	0.0762 ± 0.0006	15.38 ± 0.15	43.4	2.0 ± 0.3	0.031
PP-S_u −1	40.0 ± 0.2	0.0747 ± 0.0009	15.43 ± 0.12	44.3	4.3 ± 0.2	0.300
PP-S_u −3	38.6± 0.3	0.0732 ± 0.0010	15.90 ± 0.16	45.2	6.6 ± 0.3	0.320
PP-S_u −5	38.5 ± 0.2	0.0717 ± 0.0008	16.30 ± 0.11	46.1	7.6 ± 0.2	0.406
PP-S_u −7	34.8 ± 0.3	0.0657 ± 0.0007	16.63 ± 0.18	49.8	15.0 ± 0.3	0.522
PP-S_t −0.5	41.8± 0.2	0.0743 ± 0.0010	15.53 ± 0.12	44.5	2.7 ± 0.2	0.029
PP-S_t −1	40.6 ± 0.3	0.0732 ± 0.0009	16.48 ± 0.15	45.2	4.6 ± 0.3	0.120
PP-S_t −3	39.2 ± 0.4	0.0715 ± 0.0006	17.25 ± 0.14	46.2	7.1 ± 0.4	0.128
PP-S_t −5	37.9 ± 0.2	0.0700± 0.0009	17.43 ± 0.17	47.2	9.2 ± 0.2	0.130
PP-S_t −7	34.7 ± 0.4	0.0663 ± 0.0008	17.60 ± 0.11	49.5	14.8 ± 0.4	0.223
PP-PPgMA-5-S_u −5	38.0 ± 0.2	0.0654 ± 0.0007	17.00 ± 0.09	50.0	12.0 ± 0.2	0.694
PP-PPgMA-5-S_t −5	38.4 ± 0.3	0.0640 ± 0.0009	18.03 ± 0.11	50.9	12.5 ± 0.3	0.619

[a]Degree of crystallinity based on MDSC measurements.
[b]Loss factor based on DMA analyses.
[c]Glass transition temperature evaluated through DMTA.
[d]Constrained phase [19].
[e]Amorphous constrained phase.
[f]Brittleness determined according to [25, 26].

untreated and treated silica. The addition of the compatibilizer resulted in a significant increase of the normalized storage modulus above T_g especially for the composites containing untreated silica particles. As it is expected, the silica particle dispersion becomes more homogeneous upon the addition of PPgMA which means that there are fewer or/and smaller agglomerates. Thus, there is more silica surface available to interact with the polymer resulting in immobilization of more polymer chains and larger constrained polymer phase. Noteworthy, the brittleness was quantitatively determined according to a recent model proposed by Brostow et al. [25, 26] which takes into account the tensile elongation at break and the storage modulus determined by DMA at 25°C. The brittleness increases with the filler content for both PP-S_u and PP-S_t composites (Table 1), showing lower increase in the case of PP-S_t composites because of the lower degree of agglomeration and more homogeneous distribution of silica particles that limits the decrease in elongation at break as compared with PP-S_u composites (see paragraph 3.4). Incorporation of PPgMA improves the filler dispersion and distribution but also intensifies the polymer/filler interfacial interactions, determining a significant decrease in elongation and a correspondent increase in brittleness.

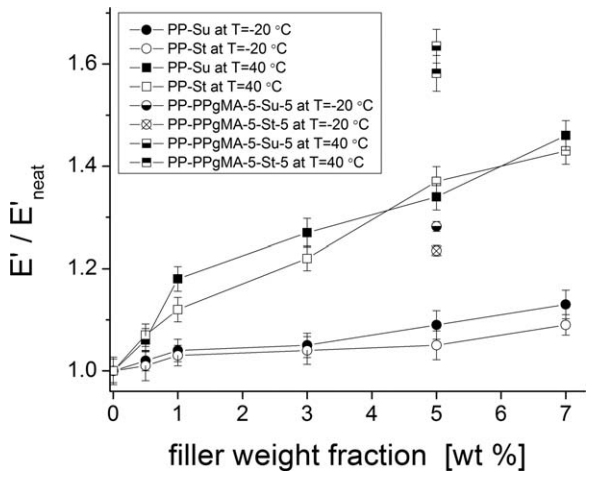

FIG. 2. Normalized storage modulus evaluated below and above the glass transition temperature as a function of filler content.

The degree of crystallinity χ, is determined as a function of the silica type and amount according to *Eq. 1* and by accounting for the weight fraction of PP in the composite (W_{PP}) as:

$$\chi = \frac{\Delta H}{\Delta H_m^* \ (W_{PP})} \ 100 \qquad (1)$$

where ΔH_m^* is the melting enthalpy of 100% crystalline isotactic PP equal to 209 J/g [27].

As shown in Table 1, the degree of crystallinity decreases upon addition of silica irrelevant of the silica type or the presence of compatibilizer, probably due to the fact that the polymer chains, during crystallization in the molten state, are immobilized at the silica surface.

In particular, the fraction of polymer chains anchored at the filler surface dictates the interfacial interactions between the filler and matrix and can be determined by investigating the thermomechanical behavior of the nanocomposites as a function of filler content and temperature. The fraction of the constrained region, C, is estimated by applying a peculiar theoretical model specifically developed for semicrystalline polymers [28]. This model takes into account a constrained region formed by the crystalline phase and also part of the amorphous phase that was immobilized at the crystal surface upon crystallization, whereas the rest of the amorphous phase is considered as mobile phase. The model was modified to be applied for polymer nanocomposites by considering that the amorphous phase

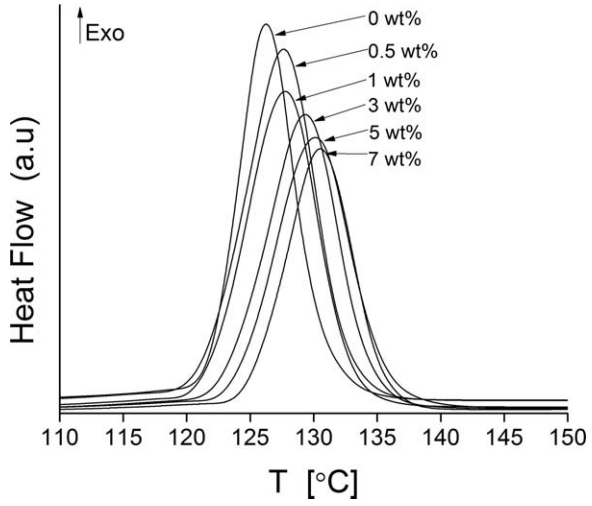

FIG. 3. Representative curves describing the nonisothermal crystallization behaviour of PP-S_u composites for increasing filler contents.

can be immobilized not only on the crystal surface but also on the filler surface [19]. Therefore, the constrained phase *C* represents the polymer crystalline phase and amorphous phase immobilized at the crystal and filler surface, whereas the mobile phase consists only of amorphous polymer chains. Because the constrained region does not contribute to the energy loss, it can be expressed in terms of the energy loss ratio of the composite and neat polymer at T_g, W_c, and W_0, respectively, and χ which is the degree of crystallinity for the pure PP (*Eq. 2*). The degree of crystallinity along with the tan δ values at T_g, reported also in Table 1.

$$C = 1 - \frac{W_c}{W_0}(1-\chi) \tag{2}$$

where the energy loss ratio *W* is defined as:

$$W = \frac{\pi \tan\delta}{(\pi \tan\delta + 1)} \tag{3}$$

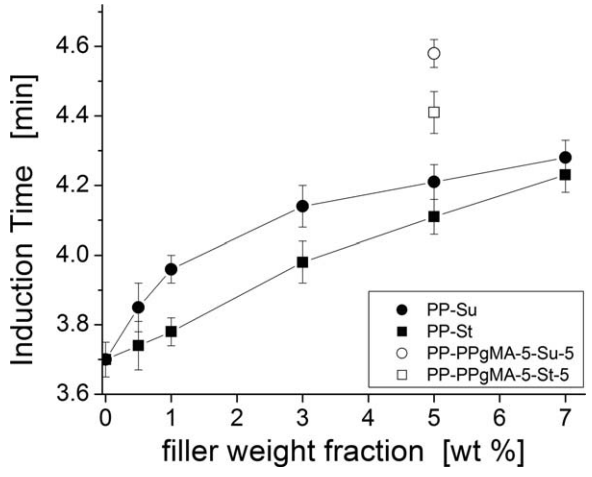

FIG. 4. Crystallization induction time, obtained from the nonisothermal DSC crystallization curves, as a function of the filler content.

It is noted that the constrained phase consists of polymer crystalline phase and amorphous polymer chains immobilized at the silica surface and does not contribute to loss or dissipated energy. The fraction of the amorphous immobilized phase (C-χ), shown also in Table 1, can be found by subtracting the degree of crystallinity χ from the overall constrained phase *C*.

The nonisothermal crystallization behavior, as studied by MDSC, showed that the onset crystallization temperature (i.e., characterizing the beginning of the crystallization) increases with the silica content (Fig. 3), indicating that the filler is acting as a nucleating agent as reported also elsewhere [29]. Therefore, the crystallization induction time (Δt_i), defined as the time difference between onset and endset time of the crystallization, was found to increase with the filler content as shown in Fig. 4, indicating that the polymer chains have longer time to rearrange forming more perfect and/or thicker crystals as reported also in a previous work [30]. Moreover, in the same article, it was shown that the crystallization rate of PP-silica nanocomposites under isothermal or nonisothermal condition was significantly increased, indicating a remarkable nucleating action of silica fillers (i.e., more surfaces are available for nucleation of new crystals). Overall, the observed crystallization behavior indicates that a transcrystalline phase forms on the filler surface during crystallization. The composites containing compatibilizer exhibited even greater values of induction time, due to the larger silica surface available to interact with the polymer chains.

In conclusion, the silica–polypropylene interfacial interactions, assessed through the viscoelastic and crystallization properties of the composites, lead to the formation of a complex polymer phase constrained at the silica surface that consists of both amorphous polymer chains and polymer crystalline region in the form of transcrystalline zone.

Correlation Between Tensile and Viscoelastic Properties

The tensile elastic modulus and T_g, determined as a function of the silica type and content, follow a similar trend as shown in Fig. 5. In particular, both properties increase with filler content up to ~1 wt%, reach a plateau for 1–3 wt% and continue to increase at higher filler content in case of the untreated silica (S_u) composites. This nonmonotonical trend indicates the presence of two competing effects, the stiffening effect due to the high modulus of silica particles (E ~ 70 GPa) and the formation of silica aggregates due to poor dispersion within the matrix. On the other hand, the properties of the silica treated (S_t) composites manifested a monotonical trend characterized by a greater increase at low filler content and a plateau at higher filler amounts. The higher reinforcing efficiency of S_t indicates better dispersion.

Moreover, the addition of PPgMA results in a significant increase in T_g but limited enhancement in elastic

 DOI 10.1002/pc

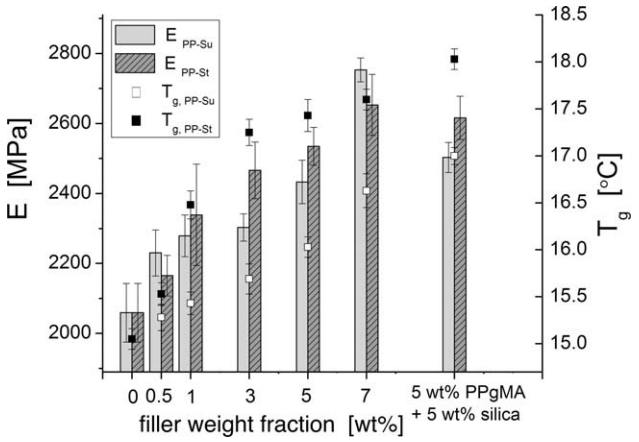

FIG. 5. Tensile elastic modulus and T_g obtained from DMA of PP-S_u and PP-S_t composites as a function of the filler content.

modulus for both PP-S_u and PP-S_t composites. This behavior can be ascribed to the low molecular weight of the compatibilizer as compared with PP, which limits the improvement in bulk mechanical properties, and to the effect of compatibilization in promoting stronger filler–matrix interactions which are reflected in local physical properties such as T_g. As expected, the addition of PPgMA has lower impact in treated silica composites whose filler–matrix interfacial interactions have been already strengthened because of the filler surface treatment (see T_g data in Table 1).

The correlation of tensile modulus to T_g provides understanding on the reinforcing mechanisms which contribute to the enhancement of the tensile and viscoelastic properties. Specifically, the increase of both properties is mainly due to the reinforcing effect of the high modulus silica filler [31, 32]. Moreover, as changes in T_g are related to the primary relaxation of polymer chains and the extent of the immobilized chains, the alteration of polymer chain mobility upon nanofiller addition also contributes to the enhancement of the properties as reported also in [33, 34]. Other secondary effects, such as the change in polymer's crystallinity and crystal structural forms, may also contribute to the reinforcing action of silica nanoparticles [35, 36]. Noteworthy, a qualitatively correlation between elastic modulus and T_g can be observed in Fig. 6 for PP-S_u and PP-S_t composites for increasing filler contents (from 0 to 7 wt%). Interestingly, the increase in elastic modulus is accompanied by a correspondent increase in T_g in the case of PP-S_t composites. The experimental data points evidence a trend that can be qualitatively described using a polynomial function of the second order. Moreover, the concave trend seems more pronounced in the case of PP-S_u composites, probably due to the presence of two competing effects mentioned earlier (stiffening effect and the formation of silica aggregates).

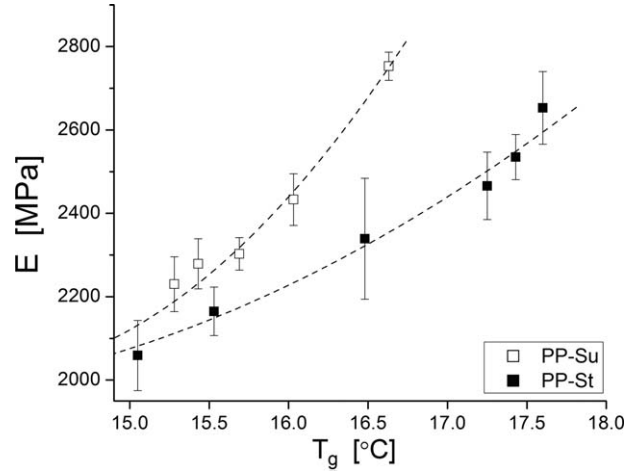

FIG. 6. Tensile elastic modulus as a function of the T_g obtained from DMA of PP-S_u and PP-S_t composites for increasing filler contents (from 0 to 7 wt%). The data points have been fitted using a polynomial function of the second order.

Correlation of Interfacial Interactions to Tensile and Viscoelastic Properties

The interfacial interactions were assessed indirectly and the macroscopic properties, that is, tensile modulus, were correlated to the viscoelastic properties, that is, T_g, which are dictated by the interfacial interactions [37]. The question that remains to be addressed is whether the interfacial interactions can be described in a more quantitative way using the experimentally determined tensile and viscoelastic properties. Two theoretical models, the one proposed by Pukanszky [21] and the one proposed by Sumita et al. [22], that related the tensile and viscoelastic properties, respectively, with the interfacial interactions are used in this study.

The Pukanszky model [21] is described by *Eq. 4* below:

$$\frac{\sigma_{y,c}}{\sigma_{y,m}} = \frac{1-\phi}{1+2.5\phi}\exp(B_P\phi) \tag{4}$$

where $\sigma_{y,c}/\sigma_{y,m}$ is the ratio of the yield stress of the nanocomposites to that of the neat polymer, and ϕ is the filler volume fraction. It is noted that the fraction $[(1-\phi)/(1+2.5\phi)]$ takes into consideration the decrease of the effective load-bearing cross-section, whereas the exponential represents all other effects resulting in an increase of the yield stress [20]. B_P is a parameter that accounts for the interface and interphase properties, with larger B_P values corresponding to stronger interfacial adhesion and is given by *Eq. 5* [38]:

$$B_P = \left(1+\tau\ \rho_f\ S_f\right)\ln\left(\sigma_{y,i}/\sigma_{y,m}\right) \tag{5}$$

where τ is the thickness of the interphase, ρ_f, S_f are the density and specific surface area of the filler and $\sigma_{y,i}$ is the yield stress of the interphase, respectively. Because of technical challenges, it is really cumbersome if possible at all to experimentally and reliably determine the

thickness and yield stress of the interphase, so the parameter B_P can be determined using *Eq. 4*, considering that all the other parameters in that equation can be easily determined experimentally.

The model proposed by Sumita et al. [22] relates the viscoelastic properties to the interfacial interactions and is described by *Eq. 6*:

$$\frac{E_c''}{E_m''} = (1-\phi_e)^{-1} = (1-\phi\ B_s)^{-1} \tag{6}$$

where (E_c''/E_m'') is the ratio of the loss modulus of the nanocomposites to that of the neat polymer, ϕ_e is the effective volume fraction of the dispersed phase defined as the volume of filler (ϕ) plus that of the "constrained matrix" associated with the interface and B_S is a parameter describing the relative value of the effective volume per single particle. The two parameters B_P and B_S, which are directly related to how strong the interface/interphase is, are presented in Fig. 7a as a function of the filler volume fraction ϕ for PP-S_u and PP-S_t composites. For both composite types, B_P and B_S increase up to a threshold volume fraction value of ~0.5–0.7 vol% (correspondent to ~1–1.5 wt%) and decrease at higher volume fractions. This trend indicates that the polymer/filler interfacial adhesion is enhanced up to the threshold value, whereas the higher concentration of aggregates at greater filler contents leads to a significant decrease in the average specific surface area of silica particles, resulting in a decrease of the B parameters as reported also in Ref. [20]. Specifically, when passing the threshold filler content, the value of ϕ_e increases less rapidly with further addition of particles, as determined by *Eq. 6* and shown in Fig. 7b, indicating that the thickness of the physically absorbed PP layer on the surface of the silica particles is limited due to agglomeration [38]. Moreover, the effective volume per single particle (B_S parameter) continuously decreases, indicating that the extent of the particle agglomeration also increases with filler content. Higher B values are obtained for PP-S_t than for PP-S_u composites, as expected due to better dispersion of the treated silica particles. Moreover, the difference of the B values of the two composite types becomes significantly less at higher silica contents when aggregates are present irrelevant of the type of silica used. Composites containing compatibilizer (i.e., PP-PPgMA-5-S_u−5 and PP-PPgMA-5-S_t−5) show higher values in B values and ϕ_e, indicating a better filler dispersion and/or an increase in interphase thickness. When considering the quantities involved in the Pukanszky and Sumita models, the similar trend followed by B_P and B_S parameters, a strong correlation between the macroscopic tensile properties and viscoelastic properties can be clearly observed. In addition, a similar trend can also be recognized between elastic modulus, T_g and ϕ_e, providing further evidence of the presence of secondary reinforcing mechanisms in silica nanocomposites. Finally, a comparable trend can be identified between the amount of constrained amorphous phase (C-χ) and the effective volume fraction of the dispersed phase (ϕ_e) as shown in Fig. 7c.

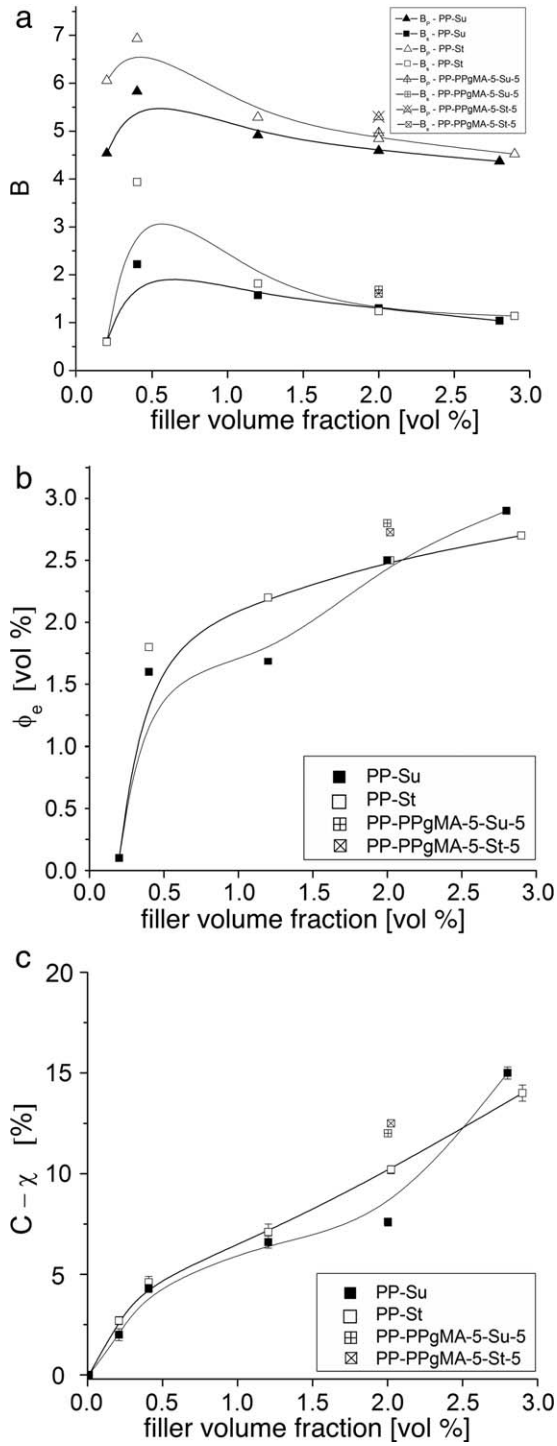

FIG. 7. Plot of (a) the B parameters, (b) the effective volume fraction of the dispersed phase ϕ_e and (c) the immobilized amorphous phase (C-χ) as a function of the filler volume content.

Morphology Characterization

SEM micrographs of fracture surfaces for PP nanocomposites loaded with 5 wt% silica are shown in Fig. 8. Silica aggregates appear distributed inhomogeneously

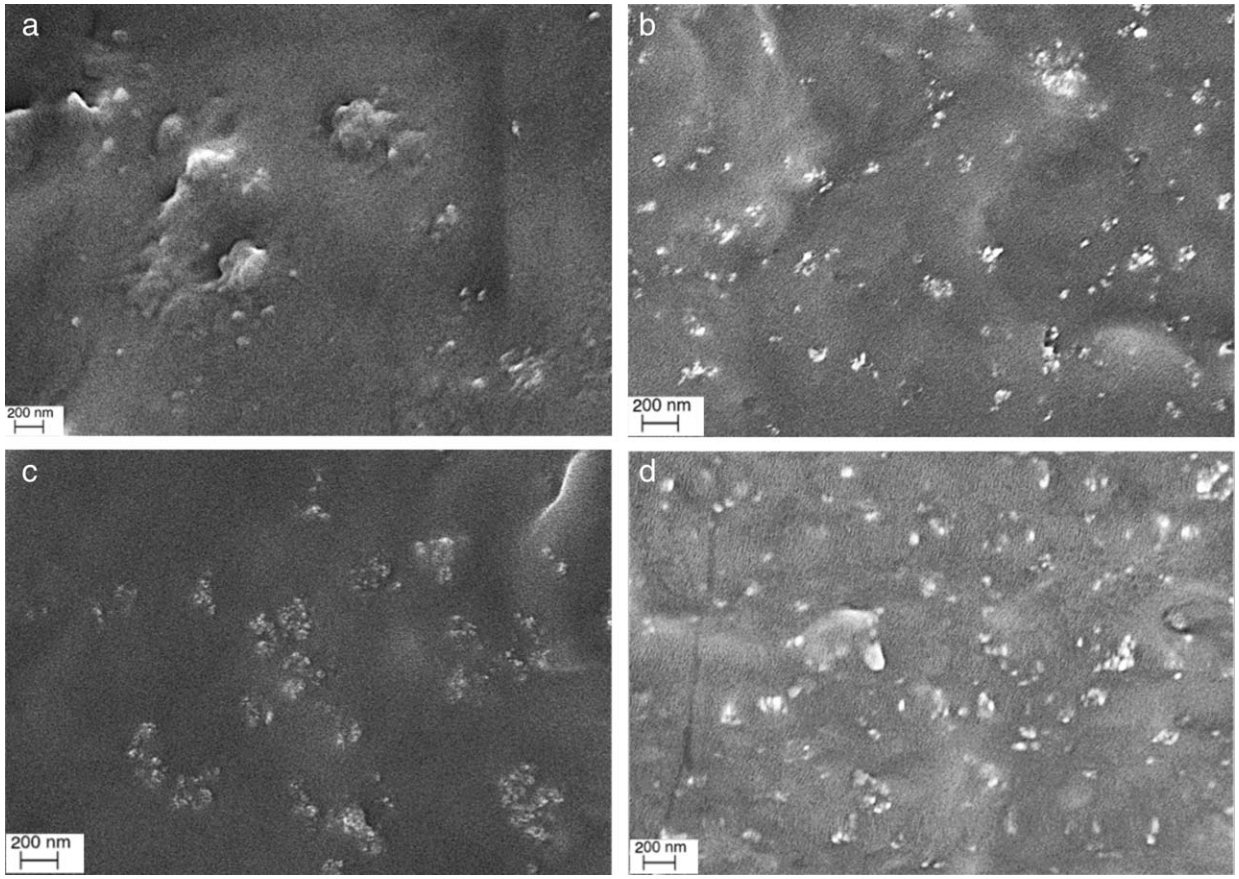

FIG. 8. SEM micrographs of fracture surfaces of (a) PP-S_u-5, (b) PP-S_t-5 (c) PP-S_u-7 and (d) PP-S_t-7.

within the matrix in PP-S_u-5 nanocomposite (Fig. 8a). On the other hand, the incorporation of surface-treated silica seems to promote a better dispersion of the filler and the size of aggregates is markedly lower (Fig. 8b). Moreover, the smaller aggregate dimensions observed in PP-S_t-5 composites can substantiate the better tensile and viscoelastic mechanical properties when compared to PP-S_u-5 sample (Fig. 1). The composite filled with 7 wt% of untreated silica presents rather poorly dispersed silica particles organized in aggregates and agglomerates with average dimension of around 250 nm (Fig. 8c), while the homogeneous distribution of relatively small silica aggregates is maintained in composites filled with 7 wt% of untrated silica (Fig. 8d). The microstructural observations confirm that higher filler contents leads to reduced interfaces, resulting in a lower efficiency in improving the mechanical properties.

CONCLUSIONS

This study focused on understanding the interfacial interactions between nanosilica and polypropylene and their effect on the physical and macroscopic properties of PP-silica nanocomposites. The tensile modulus and strength of the composites were determined as a function of the filler content (up to 7 wt%) and type of silica particles (untreated vs. treated). To understand how the filler–matrix interfacial interactions are affecting the tensile and viscoelastic properties of the composite, different models dealing with the static and dynamic mechanical behavior of the particulate composites were applied. The Pukanszky's model, used to correlate the composite's strength with the interfacial strength, was shown to ascertain the influence of the filler surface functionalization on the intensity of the interfacial interactions. It was found that stronger interfacial interactions are established in the compatibilized silica nanocomposites. The Sumita's model, used to correlate the normalized loss modulus with the interfacial strength, was found to follow a qualitatively similar trend.

A significant correlation between the tensile modulus, glass transition temperature and the amount of constrained polymer phase at the silica surface, as assessed through tensile and DMA analyses, revealed the presence of a secondary reinforcing mechanism, which, concurrently to the primary stiffening effect of the high modulus filler, contributes to the enhancement of the nanocomposites bulk properties. The polymer constrained phase, responsible for providing a secondary reinforcing mechanism, was thus modeled as immobilized amorphous and transcrystalline polymer regions located at the filler surface.

ACKNOWLEDGMENTS

The authors thank Mr. Matthew Smith from the School of Materials Science and Engineering at the Georgia Institute of Technology for helping with the morphological observations.

REFERENCES

1. F. Hussain, *J. Compos. Mater*., **40**, 1511 (2006).
2. L.S. Schadler, L.C. Brinson, and W.G. Sawyer, *Nanocompos. Mater*., **59**, 53 (2007).
3. A. Fina, D. Tabuani, and G. Camino, *Eur. Polym. J*., **46**, 14 (2010).
4. S. Kim, I. Do, and L.T. Drzal, *Macromol. Mater. Eng*., **294**, 196 (2009).
5. D. Pedrazzoli, A. Dorigato, and A. Pegoretti, *J. Nanosci. Nanotechnol*., **12**, 4093 (2012).
6. R. Qiao and L. Catherine Brinson, *Compos. Sci. Technol*., **69**, 491 (2009).
7. Q. Yuan and R.D.K. Misra, *Mater. Sci. Technol*., **22**, 742 (2006).
8. H. Mirzazadeh, A.A. Katbab, and A.N. Hrymak, *Polym. Adv. Technol*., **22**, 863 (2011).
9. R.F. Gibson, *Compos. Struct*., **92**, 2793 (2010).
10. M.A. Bhuiyan, R.V. Pucha, J. Worthy, M. Karevan, and K. Kalaitzidou, *Compos. Struct*., **95**, 80 (2013).
11. W. Evans, R. Prasher, J. Fish, P. Meakin, P. Phelan, and P. Keblinski, *Int. J. Heat Mass Transfer*, **51**, 1431 (2008).
12. W.S. Gutowski, *J. Adhes*., **79**, 445 (2003).
13. M.A. Bhuiyan, R.V. Pucha, M. Karevan, and K. Kalaitzidou, *Comput. Mater. Sci*., **50**, 2347 (2011).
14. H. Liu and L.C. Brinson, *Compos. Sci. Technol*., **68**, 1502 (2008).
15. B. Pukánszky, *Eur. Polym. J*., **41**, 645 (2005).
16. I.M. Kalogeras and H.E. Hagg Lobland, *J. Mater. Educ*., **34**, 69 (2012).
17. T. Ramanathan, S. Stankovich, D.A. Dikin, H. Liu, H. Shen, S.T. Nguyen, and L.C. Brinson, *J. Polym. Sci. Part B: Polym. Phys*., **45**, 2097 (2007).
18. T.H. Zhou, W.H. Ruan, J.L. Yang, M.Z. Rong, M.Q. Zhang, and Z. Zhang, *Compos. Sci. Technol*., **67**, 2297 (2007).
19. M. Karevan and K. Kalaitzidou, *Polymer*, **54**, 3691 (2013).
20. N. Aït Hocine, P. Médéric, and T. Aubry, *Polym. Test*., **27**, 330 (2008).
21. B. Pukanszky, B. Turcsanyi, and F. Tudos, "Effect of Interfacial Interaction on the Tensile Yield Stress of Polymer Composites in Interfaces in Polymer," in *Ceramic and Metal Matrix Composites*, H. Ishida Ed., Elsevier, New York, 467 (1988).
22. M. Sumita, K.M. Tsukihi, and K. Ishikawa, *J. Appl. Polym. Sci*., **29**, 1523 (1984).
23. S.W. Shang, J.W. Williams, and K.-J.M. Soderholm, *J. Mater. Sci*., **29**, 2406 (1994).
24. A. Dorigato, A. Pegoretti, and A. Penati, *Express Polym. Lett*., **4**, 115 (2010).
25. W. Brostow, H.E. Hagg Lobland, and M. Narkis, *J. Mater. Res*., **21**, 2422 (2011).
26. W. Brostow, H.E. Hagg Lobland, and M. Narkis, *Polym. Bull*., **67**, 1697 (2011).
27. E. James, *Polymer Data Handbook*, Oxford University Press, New York, (1999).
28. Y. Kojima, A. Usuki, M. Kawasumi, A. Okada, Y. Fukushima, T. Kurauchi, and O. Kamigaito, *J. Mater. Resour*., **8**, 1185 (1993).
29. M. Garcia, G. Van Vliet, S. Jain, B.A.G. Schrauwen, A. Sarkissov, W.E. Van Zyl, and B. Boukamp, *Rev. Adv. Mater. Sci*., **6**, 169 (2004).
30. D. Pedrazzoli, A. Pegoretti, and K. Kalaitzidou, *Polym. Eng. Sci*., In press.
31. K.I. Winey and R.A. Vaia, *Mater. Res. Bull*., **32**, 314 (2007).
32. S. Fu, X. Feng, B. Lauke, and Y. Mai, *Compos. B*, **39**, 933 (2008).
33. X. Zhang and L.S. Loo, *Macromolecules*, **42**, 5196 (2009).
34. R. Qiao, H. Deng, K.W. Putz, and L.C. Brinson, *J. Polym. Sci. Part B: Polym. Phys*., **49**, 740 (2011).
35. J. Karger-Kocsis, J. Varga, and G.W. Ehrenstein, *J. Appl. Polym. Sci*., **64**, 2057 (1997).
36. J. Garbarczyk, D. Paukszta and S. Borysiak, *J. Macromol. Sci., B*, **41**, 1267 (2002).
37. A. Kopczynska and G.W. Ehrenstein, *J. Mater. Educ*., **29**, 325 (2007).
38. M.Z. Rong, M.Q. Zhang, S.L. Pan, B. Lehmann, and K. Friedrich, *Polym. Int*., **53**, 176 (2004).

 DOI 10.1002/pc